Supporting Information for

Up-conversion Intersystem Crossing Rates in Organic Emitters for Thermally Activated Delayed Fluorescence (TADF): Impact of the Nature of Singlet vs. Triplet Excited States

Pralok K. Samanta,[†] Dongwook Kim,[*,†,‡] Veaceslav Coropceanu,[§] and Jean-Luc Brédas[*,†]

[†]Laboratory for Computational and Theoretical Chemistry of Advanced Materials

Physical Science and Engineering Division

King Abdullah University of Science and Technology

Thuwal 23955-6900, Kingdom of Saudi Arabia

[‡]Department of Chemistry

Kyonggi University

154-42 Gwanggyosan-Ro, Yeongtong-Gu, Suwon 440-760, Korea

[§]School of Chemistry and Biochemistry

Center for Organic Photonics and Electronics (COPE)

Georgia Institute of Technology

Atlanta, Georgia 30332-0400

*E-mail: dongwook-kim@kyonggi.ac.kr, jean-luc.bredas@kaust.edu.sa

Contents

1. Theoretical Backgrounds

1. Optical Excitation

The excitation energies are calculated within the Tamm-Dancoff Approximation (TDA) with the 6-31+G(d) basis set. The recent development of optimally tuned range-separated (OT-RS) exchange functional allows the reliable calculations of the charge-transfer (CT) excited-state properties of molecules or complexes.[1-6] In range-separated exchange-correlation functional, the Coulomb operator is split into local and non-local regions:

$$\frac{1}{r_{12}} = \frac{1-\mathrm{erf}(\omega r_{12})}{r_{12}} + \frac{\mathrm{erf}(\omega r_{12})}{r_{12}} \qquad \text{(S1)}$$

The range-separation parameter ω determines where the exchange term switches from short-range region (DFT exchange) to the long-range region (Hartree-Fock exchange). The ω value is optimized based on the principle that the vertical ionization potential (IP_v) must be equal to the negative of the HOMO energy (ε_H) in exact Kohn-Sham (KS) or generalized KS (GKS) theory;[7] for the gap-tuned functionals, the optimal ω value is obtained by minimizing the J^2 value:[3, 8-9]

$$J^2 = \sum_{i=0}^{1}[\epsilon_H(N+i) + IP(N+i)]^2 \qquad \text{(S2)}$$

The optimal ω values for the LC-ωPBE functional are listed in Table S4 for all the molecules considered in this study. Note that we refer to the LC-ωPBE functional with the optimal ω value as LC-ω*PBE.

2. Local excitation (LE) vs charge transfer (CT) contributions

The Natural Transition Orbital (NTO) analysis of a given excited state can be conducted *via* the singular-value decomposition of the 1-particle transition density matrix, **T**, *i.e.*,

$$\left|\left(\mathbf{U}^{\dagger}\mathbf{T}\mathbf{V}\right)_{ij}\right| = \delta_{ij}\alpha_i \qquad \text{(S3)}$$

where α is the singular value; δ_{ij} is the Kronecker delta; **U** and **V** are unitary square matrices that transform the canonical occupied and virtual molecular orbitals (MOs) into hole and particle NTOs, respectively. The Löwdin population on atom μ for the hole and electron NTOs can be given using the density matrix for the NTOs, $\mathbf{D_{NTO}}$, *i.e.*,

$$P_{NTO}^{\mu} = \sum_{i\in\mu}\left(\mathbf{S^{1/2}}\mathbf{D_{NTO}}\mathbf{S^{1/2}}\right)_{ii} \qquad \text{(S4)}$$

where **S** is the overlap matrix in the AO basis; $\mathbf{D_{NTO}} = \mathbf{C_{NTO}^{\dagger}}\mathbf{C_{NTO}}$, and $\mathbf{C_{NTO}}$ denotes a coefficient matrix for either a hole or electron NTO in the AO basis, respectively. The local-excitation (LE) and charge-transfer (CT) contributions to a given excited state are computed as:

$$f = \sum_{i=1}^{Nocc}\alpha_i^2 P_{hNTO}^{\mu} P_{eNTO}^{\nu} \qquad \text{(S5)}$$

When atoms μ and ν belong to the same fragment, the f value above points to the LE contribution to the state; otherwise, it is related to CT contribution.

3. Extent of overlap between hole and electron wave functions

The extent of overlap between the hole and electron wave function, ξ, is calculated using Multiwfn-3.3.8:[10]

$$\xi = \int \min(\rho_h(\boldsymbol{r}), \rho_e(\boldsymbol{r}))\, d\boldsymbol{r} \qquad \text{(S6)}$$

where $\rho_h(\mathbf{r})$ and $\rho_e(\mathbf{r})$ are the density of hole and electron, respectively, at position **r**.

4. Singlet-triplet Energy Gap, ΔE_{ST}

Figure S1(a) shows the comparison between the experimental and computational values of ΔE_{ST} for all the molecules studied in this report. As the theoretical results appear to be reliable, we can base our discussion on the theoretical values.[8] As mentioned earlier, the overlap between the hole and electron wave functions can be taken qualitatively as a measure of K.[11] Thus, in Figure S1(b), we also plotted the calculated ΔE_{ST} values as a function of the sum of the overlaps between the hole and electron NTOs for both S_1 and T_1 states. The correlation is rather poor, which again reflects the fact that the molecules often have singlet and triplet excited states of different characters, and hence K is not the sole factor determining ΔE_{ST}. It is thus desirable to gain a better understanding of the factors governing ΔE_{ST}.

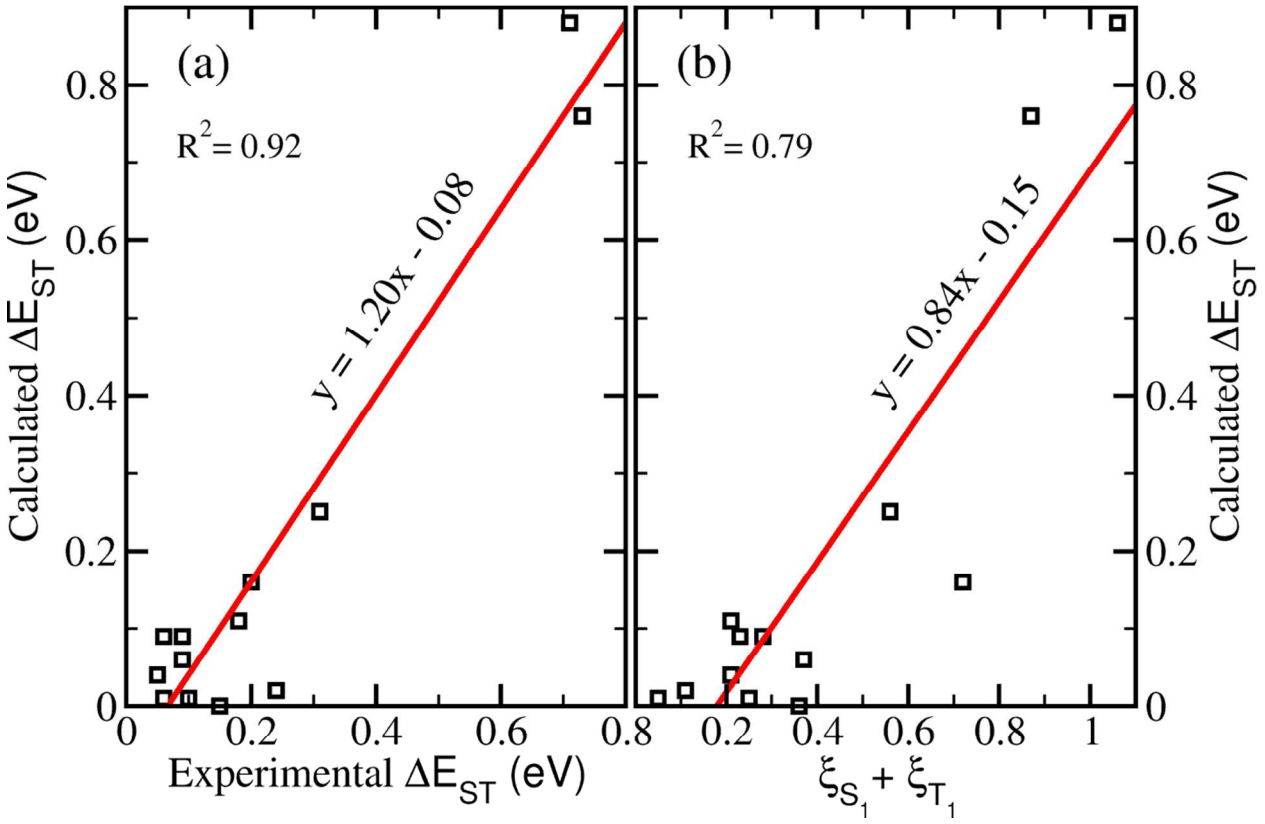

Figure S1. (a) Comparison between experimental and computational values of ΔE_{ST}; (b) ΔE_{ST} as a function of the sum of the overlaps between hole and electron wave functions (ξ) in the S_1 and T_1 states (ξ_{S_1} and ξ_{T_1} are calculated at the optimized geometries of the respective states; see Table S1) for all the molecules studied in this report.

5. *Reorganization energy*:

In the evaluation of k_{UISC} (see Eqs 1 and 2) the reorganization energy (λ) and related Huang-Rhys factors must be estimated. The reorganization energy can be represented as a sum of the contributions from the surroundings, λ_s, and those from intramolecular vibrations, λ_{intra}. The latter can be defined as:

$$\lambda_{\text{intra}} = E^*_{S_1} - E^0_{S_1} \qquad \text{(S7)}$$

where $E^*_{S_1}$ is the S_1 state energy at the T_1-state (or sometimes T_2-state) geometry, and $E^0_{S_1}$ is the one at the S_1-state geometry. We note that λ_{intra} can be divided into a part arising from low-frequency modes, which can be treated in a classical way, and a part associated with high-frequency modes.[12-13] The sum of reorganization energy due to intramolecular low-frequency vibrations and that from surroundings (λ_s) is denoted in Eq. 2 as λ_M. Many high-frequency modes, in general, contribute to the reorganization energy. In Marcus-Levich-Jortner model, in order to simplify the calculations of the Franck-Condon-weighted density of states (Eq. 2) the effect of all contributing modes is represented via an effective mode with an effective frequency, ω_{eff}, and effective Huang-Rhys factor, S_{eff}.

Upon an electronic transition, the geometry of the system changes via vibrational relaxations. The total intramolecular reorganization energy, λ_{intra}, can be represented as a sum of contributions from individual vibrational normal modes, i, as:

$$\lambda_{intra} = \sum \lambda_i = \sum \hbar \omega_i S_i \qquad \text{(S8)}$$

$$\lambda_i = \frac{k_i}{2} \Delta Q_i^2 \qquad \text{(S9)}$$

$$S_i = \frac{\lambda_i}{\hbar\omega_i} \qquad \text{(S10)}$$

where k_i and ΔQ_i denote the force constant for the normal mode i and the coordinate displacement from the T_1-state equilibrium position to the S_1-state one along the mode i, respectively.

The $\omega_{eff,}$ and S_{eff} are obtained by means of Eqs. (S11) and (S12) where the summation is performed only over the high-frequency vibrational modes (not included in $\lambda_{M.}$):[14]

$$\hbar\omega_{eff} = \frac{\sum \hbar\omega_j S_j}{\sum S_j} \qquad \text{(S11)}$$

$$S_{eff} = \sum S_j \qquad \text{(S12)}$$

For example, in case of 2CzPN we found three vibrational normal modes with significant S values. The frequencies of such normal modes are 1543, 1564, and 1574 cm^{-1}, and S factors for those modes are 0.10, 0.03 and 0.23, respectively. Thus the computed effective normal mode is 1565 cm^{-1} (0.19 eV) and effective S is calculated to be 0.36.

On the other hand, a vibrational mode is determined to be low-frequency one if its energy is smaller than the thermal energy. We found that such modes correspond to the one less than ca. 200 cm^{-1} at 300 K and the associated S factors are less than 0.1. Hence, their contribution to λ would be very small; for example, given the thermal energy of ca. 26 meV at 300K and S factor of 0.1, the contribution from the low-frequency mode of ca. 200 cm^{-1} is approximately 2.6 meV.

For a few representative molecules, the vibration relaxation energy of the S_1 state and the associated *S* factor were calculated using the DUSHIN program developed by Reimers.[15] The computed effective reorganization energies due to high-frequency, nonclassical intramolecular vibrations ($S \cdot \hbar\omega_{eff}$) are found to be in the range of 0.01 eV to 0.19 eV (Table S2). Thus, overall, the Marcus reorganization energy due to low-frequency intramolecular vibrations and the surrounding medium-induced relaxations can be expected to fall in the range ~0.1-0.2 eV.[13, 16] Given that a rigorous evaluation of λ_M values for the large molecules in our study would be a difficult task, we simply considered effective values of 0.1 and 0.2 eV for λ_M in the calculation of the k_{UISC} rates. In addition, the high-frequency effective reorganization energy ($S \cdot \hbar\omega_{eff}$) turned out to have only limited impact. For instance, in the case of 2CzPN for which the $S \cdot \hbar\omega_{eff}$ value is 0.07 eV (Table S2), k_{UISC} with and without taking high-frequency modes into account are estimated to be 2.1×10^3 s^{-1} and 3.0×10^3 s^{-1}, respectively, when λ_M is set as 0.1 eV; similarly, in the case of PXZ-TRZ for which $S \cdot \hbar\omega_{eff}$ is even larger (0.19 eV), the corresponding rates are 1.4×10^7 s^{-1} and 3.2×10^7 s^{-1}, with the same λ_M; see Table S3. Such small differences overall mean that the impact of *S* can be neglected in the evaluation of k_{UISC} for the molecules where *S* was not explicitly computed.

Table S1. Calculated Overlap (ξ) of Hole and Electron Wave Functions in the S_1 and T_1 states at Various Geometries.

Molecules	S_0-geometry		S_1-geometry		T_1-geometry		$\frac{\xi_{S_1}+\xi_{T_1}}{2}$ [a]
	ξ_{S_1}	ξ_{T_1}	ξ_{S_1}	ξ_{T_1}	ξ_{S_1}	ξ_{T_1}	
CBP	0.37	0.56	0.43	0.59	0.45	0.62	0.53
α−NPD	0.24	0.56	0.25	0.55	0.36	0.61	0.43
2CzPN	0.17	0.40	0.05	0.05	0.23	0.51	0.28
CC2TA	0.31	0.51	0.09	0.13	0.34	0.63	0.36
PIC-TRZ	0.19	0.38	0.08	0.11	0.09	0.11	0.10
PXZ-TRZ	0.07	0.13	0.05	0.05	0.10	0.18	0.11
ACRFLCN	0.04	0.63	0.04	0.05	0.04	0.64	0.34
Spiro-CN	0.01	0.51	0.01	0.03	0.01	0.03	0.02
4CzIPN	0.13	0.15	0.06	0.07	0.13	0.17	0.12
4CzIPN-Me	0.13	0.15	0.07	0.08	0.11	0.13	0.10
4CzPN	0.11	0.16	0.05	0.07	0.08	0.29	0.17
4CzTPN	0.12	0.17	0.11	0.15	0.17	0.25	0.18
4CzTPN-Me	0.11	0.16	0.11	0.14	0.12	0.16	0.13

[a] ξ_{S_1} [ξ_{T_1}] corresponds to the wave function overlap for the S_1 [T_1] state at the S_1- [T_1-] state geometry.

Table S2. Calculated Intramolecular Reorganization Energies (λ_{intra}) and Effective Reorganization Energies ($S \cdot \hbar\omega_{eff}$) from High-frequency Vibrations ($\hbar\omega_{eff}$) and Associated Huang-Rhys Factor (S) for Representative Molecules, in the case of Up-Conversion Intersystem Crossing (UISC).

Molecules	λ_{intra} (eV)	Huang-Rhys factor (S)	$\hbar\omega_{eff}$ (eV)	$S \cdot \hbar\omega_{eff}$ (eV)
CBP	0.077	0.08	0.21	0.017
α−NPD	0.115	0.06	0.21	0.013
2CzPN	0.243	0.36	0.19	0.068
CC2TA	0.599	--[a]	--	--
PIC-TRZ	0.011	--[a]	--	--
PIC-TRZ[b]	0.433[b]	--[a]	--	--
PXZ-TRZ	0.031	0.00	0.21	0.000
PXZ-TRZ[b]	0.389[b]	0.91[b]	0.21[b]	0.191[b]
ACRFLCN	0.004	0.00	0.20	0.000
Spiro-CN	0.003	--[a]	--	--
Spiro-CN[b]	0.400[b]	--[a]	--	--
4CzIPN	0.080	--[a]	--	--
4CzIPN-Me	0.049	--[a]	--	--
4CzPN	0.158	--[a]	--	--
4CzTPN	0.135	--[a]	--	--
4CzTPN-Me	0.049	--[a]	--	--

[a]Effective Huang-Rhys factor not taken into account, see Methodology Section in the main text.
[b]The values correspond to the transitions from the T_2 to the S_1 state.

Table S3. Comparison of the k_{UISC} (s^{-1}) Rates Calculated with and without Consideration of the Associated Huang-Rhys Factor (S), for 2CzPN and PXZ-TRZ.

Molecules	Huang-Rhys factor (S)	k_{UISC}	
		λ_M=0.10 eV	λ_M=0.20 eV
2CzPN	0.36	2.08×10^{3}	1.16×10^{4}
	0.00	2.98×10^{3}	1.67×10^{4}
PXZ-TRZ	0.91[a]	1.37×10^{7}[a]	3.91×10^{6}[a]
	0.00[a]	3.16×10^{7}[a]	8.67×10^{6}[a]

[a] The values correspond to the UISC from the T_2 to S_1 state.

Table S4. Calculated (LC-ω*PBE/6-31+G(d)) and Experimental Vertical Excitation Energies for the S_1 State, $E_{VA}(S_1)$, and Adiabatic Singlet (S_1)-Triplet (T_1) Energy Differences, ΔE_{ST}.[a]

Molecules	ω^* Bohr^{-1}	$E_{VA}(S_1)$		ΔE_{ST}	
		Calculated	Expt.[b]	Calculated	Expt.[b]
$\Delta E_{ST} > 0.70$ eV					
CBP	0.173	3.94	3.80	0.88	0.71
α-NPD	0.170	3.29	3.31	0.76	0.73
ΔE_{ST}=0.10~0.50 eV					
2CzPN	0.176	3.22	3.19	0.25	0.31
CC2TA	0.159	3.66	3.64	0.16	0.20
PIC-TRZ	0.141	3.17	3.35	0.11	0.18
$\Delta E_{ST} < 0.10$ eV					
PXZ-TRZ	0.183	2.94	2.73	0.09	0.06
ACRFLCN	0.174	3.03	3.05	0.02	0.24
Spiro-CN	0.168	2.73	2.69	0.01	0.06
4CzIPN	0.142	2.52	2.85	0.01	0.10
4CzIPN-Me	0.132	2.36	-	0.04	0.05
4CzPN	0.146	2.55	2.82	0.00	0.15
4CzTPN	0.147	2.32	2.61	0.06	0.09
4CzTPN-Me	0.143	2.28	2.49	0.09	0.09

[a]All values are in eV. [b]Experimental values are taken from Ref. 17.

Table S5. Calculated Vertical Transition Energies for the S_1 State, $E_{VA}(S_1)$, and Vertical Singlet (S_1)-Triplet (T_1) Energy Differences, $\Delta E_{ST\text{-}v}$ at the Ground-state Geometry, using Various DFT Functionals.[a]

Molecules	LC-ω*PBE		B3LYP		M06-2X	
	$E_{VA}(S_1)$	$\Delta E_{ST\text{-}v}$	$E_{VA}(S_1)$	$\Delta E_{ST\text{-}v}$	$E_{VA}(S_1)$	$\Delta E_{ST\text{-}v}$
CBP	3.94	0.66	3.52	0.50	4.04	2.23
α−NPD	3.29	0.57	2.98	0.43	3.55	2.36
2CzPN	3.22	0.41	2.79	0.27	3.52	1.90
CC2TA	3.66	0.35	3.06	0.08	4.00	2.14
PIC-TRZ	3.17	0.22	2.89	0.08	3.75	2.00
PXZ-TRZ	2.94	0.07	2.23	0.03	3.24	1.51
ACRFLCN	3.03	0.07	2.50	0.01	3.52	2.12
Spiro-CN	2.73	0.07	1.93	0.00	3.10	1.70
4CzIPN	2.52	0.12	2.36	0.10	3.09	1.56
4CzIPN-Me	2.36	0.12	2.24	0.10	2.98	1.44
4CzPN	2.55	0.13	2.34	0.15	3.15	1.70
4CzTPN	2.32	0.14	2.09	0.10	2.85	1.43
4CzTPN-Me	2.28	0.12	2.01	0.09	2.84	1.38
MAD[b]	0.00	0.00	0.39	0.09	0.43	1.57

	PBE0		BHandLYP	
	$E_{VA}(S_1)$	$\Delta E_{ST\text{-}v}$	$E_{VA}(S_1)$	$\Delta E_{ST\text{-}v}$
CBP	3.68	0.63	4.26	1.76
α−NPD	3.13	0.57	3.76	1.80
2CzPN	2.95	0.34	3.66	1.36
CC2TA	3.29	0.17	4.21	1.71
PIC-TRZ	3.09	0.19	3.94	1.62
PXZ-TRZ	2.41	0.03	3.43	0.98
ACRFLCN	2.68	0.01	3.62	1.51
Spiro-CN	2.14	0.00	3.09	1.00
4CzIPN	2.51	0.12	3.24	1.02
4CzIPN-Me	2.39	0.12	3.13	0.91
4CzPN	2.50	0.19	3.27	1.14
4CzTPN	2.25	0.11	2.98	0.85
4CzTPN-Me	2.18	0.10	2.94	0.79
MAD[b]	**0.22**	**0.05**	0.58	1.03

[a]All the values are in eV. The calculations were conducted at the COSMO(toluene)-TDDFT level with TZP basis sets using various exchange-correlation functionals; in the case of the LC–ω*PBE functional, calculations were carried out using the PCM(toluene) model with the 6-31+G(d) basis set within the Tamm-Dancoff approximation. [b]The mean absolute deviations (MAD) values were evaluated by taking the LC–ω*PBE results as reference.

Table S6. Calculated Spin-orbit Coupling Matrix Elements between the S_1 and T_1 States at the T_1 Geometry using Various DFT Functionals for Representative Molecules.[a]

Molecules	B3LYP	M06-2X	PBE0	BHandLYP
CBP	<0.01	<0.01	<0.01	<0.01
α−NPD	0.68	0.86	0.68	0.83
2CzPN	0.66	1.64	0.74	1.16
PXZ-TRZ	0.22	1.14	0.26	1.09
ACRFLCN	0.50	0.54	0.46	0.51
Spiro-CN	0.01	0.08	0.01	0.07
4CzIPN	0.23	1.10	0.27	0.83
4CzPN	0.51	1.97	0.61	1.36
4CzTPN	0.65	3.74	0.81	2.45

[a]All values are in cm^{-1}. The calculations were conducted at the COSMO(toluene)-TDDFT/TZP level.

Table S7: Natures of Representative Excited States at T_1-state Geometry as a Function of DFT Functionals and Basis Sets†

Molecules	Excited States	LC-ω*PBE/6-31+G(d)	PBE0/TZP
		Energy (eV)	Energy (eV)
CBP	S_1	3.17 (H => L)	2.89 (H => L)
	S_2	3.83 (H-1 => L)	3.43 (H-1 => L)
	T_1	2.19 (H => L)	1.95 (H => L)
	T_2	3.37 (H-1 => L)	3.14 (H-1 => L)
α-NPD	S_1	2.94 (H => L)	2.74 (H => L)
	S_2	3.36 (H-1 => L+1; H => L+1)	3.18 (H=> L+1; H-1 => L+1)
	T_1	1.95 (H => L)	1.74 (H => L)
	T_2	2.80 (H-1 => L+1)	2.65 (H-1 => L+1)
2CzPN	S_1	2.96 (H => L)	2.68 (H => L)
	S_2	3.15 (H-1 => L)	2.89 (H-1 => L)
	T_1	2.34 (H => L)	2.15 (H => L)
	T_2	2.80 (H-1 => L)	2.60 (H-1 => L)
CC2TA	S_1	3.54 (H-1 => L; H-1 => L+1)	3.27 (H -1=> L)
	S_2	3.75 (H-5 => L)	3.34 (H => L)
	T_1	2.69 (H-4 => L+1)	2.46 (H-2 => L+1)
	T_2	3.21 (H-7 => L)	3.13 (H-1 => L; H-1 => L+1)
PIC-TRZ	S_1	2.31 (H => L)	2.17 (H => L)
	S_2	2.68 (H-1 => L)	2.54 (H-1 => L)

	T_1	2.19 (H => L)	2.09 (H => L)
	T_2	2.56 (H-1 => L)	2.46 (H-1 => L)
PXZ-TRZ	S_1	2.48 (H => L)	1.98 (H => L)
	S_2	3.47 (H => L+3)	2.78 (H => L+1)
	T_1	2.34 (H => L)	1.88 (H => L)
	T_2	2.78 (H => L+3; H => L+4)	2.69 (H => L+3; H => L+4)
ACRFLCN	S_1	2.60 (H => L)	2.26 (H=> L)
	S_2	3.72 (H-1 => L)	3.44 (H-1=> L)
	T_1	2.578 (H-1 => L)	2.24 (H=> L)
	T_2	2.580 (H => L)	2.34 (H-1=> L)
Spiro-CN	S_1	2.05 (H => L)	1.56 (H => L)
	S_2	3.17 (H-1 => L)	2.56 (H-1 => L)
	T_1	2.04 (H => L)	1.56 (H => L)
	T_2	2.45 (H => L+1)	2.28 (H => L+2)
4CzIPN	S_1	2.18 (H => L)	2.13 (H => L)
	S_2	2.42 (H-1 => L)	2.35 (H-1 => L)
	T_1	2.02 (H => L)	1.96 (H => L)
	T_2	2.24 (H-1 => L)	2.18 (H-1 => L)
4CzIPN-Me	S_1	2.00 (H => L)	1.98 (H => L)
	S_2	2.24 (H-1 => L)	2.21 (H-1 => L)
	T_1	1.87 (H => L)	1.85 (H => L)
	T_2	2.08 (H-1 => L)	2.06 (H-1 => L)
4CzPN	S_1	2.34 (H => L)	2.19 (H => L)

	S_2	2.35 (H-1 => L)	2.27 (H-1 => L)
	T_1	2.08 (H => L)	1.92 (H => L)
	T_2	2.22 (H-1 => L)	2.17 (H-1 => L)
4CzTPN	S_1	2.02 (H => L)	1.93 (H => L)
	S_2	2.35 (H-1 => L)	2.21 (H-1 => L)
	T_1	1.77 (H => L)	1.70 (H => L)
	T_2	2.10 (H-1 => L)	1.97 (H-1 => L)
4CzTPN-Me	S_1	1.80 (H => L)	1.69 (H => L)
	S_2	2.09 (H-1 => L)	1.95 (H-1 => L)
	T_1	1.65 (H => L)	1.57 (H => L)
	T_2	1.95 (H-1 => L)	1.83 (H-1 => L)

[†]H and L are highest occupied molecular orbital and lowest unoccupied molecular orbital, respectively.

Table S8. Comparison of Calculated Adiabatic Singlet-Triplet Energy Differences (ΔE_{ST} in eV) using Different T_1-state Geometries Obtained from either Unrestricted DFT (UDFT) or TD-DFT calculations.

Molecules	UDFT	TD-DFT
α-NPD	0.76	077
2CzPN	0.25	0.24
CC2TA	0.16	0.15
PIC-TRZ[a]	0.11	0.10
PXZ-TRZ	0.09	0.15
4CzIPN	0.01	-0.04
4CzPN	0.00	-0.03
4CzTPN	0.05	0.06

[a] The orderings between the T_1 and T_2 states are different for UDFT and TD-DFT, which is acceptable given the negligible energy difference between them (ca. 9 meV).

Table S9. Calculated HOMO-LUMO Energy Gaps (in eV) for Representative Molecules ($\Delta E_{H\text{-}L}^{CT}$) and their Respective Moieties Associated with the Lowest Triplet LE State ($\Delta E_{H\text{-}L}^{LE}$) at their T_1-state Geometries.[a]

Molecules	$\Delta E_{H\text{-}L}^{CT}$	$\Delta E_{H\text{-}L}^{LE}$	$\Delta E_{H\text{-}L}^{CT}$/ $\Delta E_{H\text{-}L}^{LE}$
CBP	5.79	6.63	0.873
α-NPD	5.77	5.91	0.976
2CzPN	5.65	7.43	0.760
CC2TA	6.03	6.97	0.865
PIC-TRZ	5.04	6.55	0.789
PXZ-TRZ	4.88	6.86	0.711
ACRFLCN	5.25	6.56	0.801
Spiro-CN	4.44	5.70	0.779
4CzPN	5.30	7.51	0.705

[a] The calculations were performed at the LC-ωPBE/6-31G(d) level with the range-separation parameter ω set at 0.17 $bohr^{-1}$; this is the mean value over all the molecules (among which the actual tuned ω values vary from 0.141 to 0.183). We note that the exact $\Delta E_{H\text{-}L}$ values depend on ω.

Table S10. Calculated Vertical Excitation Energies (in eV) at the Ground-state Geometries Using the Tamm-Dancoff Approximation with the LC-ω*PBE Functional, 6-31+G(d) Basis Set, and PCM Model (ε=2.37).

CBP		α-NPD		2CzPN		CC2TA		PIC-TRZ	
State	Energy	State	Energy	State	Energy	State	Energy	State	Energy
T_1	3.28	T_1	2.72	T_1	2.81	T_1	3.30	T_1	2.95
T_2	3.37	T_2	2.74	T_2	3.04	T_2	3.32	T_2	2.96
T_3	3.37	T_3	2.96	S_1	3.22	T_3	3.32	T_3	3.07
T_4	3.47	S_1	3.29	S_2	3.30	T_4	3.33	T_4	3.07
T_5	3.47	T_4	3.34	T_3	3.42	T_5	3.41	T_5	3.13
T_6	3.75	S_2	3.35	S_3	3.68	T_6	3.42	S_1	3.16
S_1	3.94	T_5	3.44			S_1	3.65	T_6	3.17
T_7	4.00	T_6	3.45			S_2	3.78	T_7	3.17
T_8	4.01							S_2	3.23
T_9	4.05								
S_2	4.05								

PXZ-TRZ		ACRFLCN		Spiro-CN		4CzIPN		4CzIPN-Me	
State	Energy	State	Energy	State	Energy	State	Energy	State	Energy
T_1	2.87	T_1	2.96	T_1	2.66	T_1	2.40	T_1	2.24
S_1	2.94	T_2	3.02	T_2	2.70	S_1	2.52	S_1	2.36
T_2	2.95	S_1	3.03	S_1	2.71	T_2	2.53	T_2	2.39
T_3	3.36	T_3	3.36	T_3	2.97	T_3	2.67	T_3	2.50
T_4	3.38	T_4	3.46	T_4	3.06	T_4	2.68	T_4	2.55
T_5	3.47	S_2	3.98	T_5	3.24	T_5	2.72	T_5	2.57
S_2	3.61			T_6	3.26	S_2	2.75	S_2	2.59
S_3	3.74			S_2	3.29				

4CzPN		4CzTPN		4CzTPN-Me	
State	Energy	State	Energy	State	Energy
T_1	2.42	T_1	2.18	T_1	2.16
T_2	2.44	S_1	2.32	T_2	2.18
S_1	2.55	T_2	2.42	T_3	2.26
S_2	2.61	T_3	2.49	S_1	2.28
T_3	2.63	T_4	2.53	S_2	2.29
		S_2	2.55	S_3	2.36

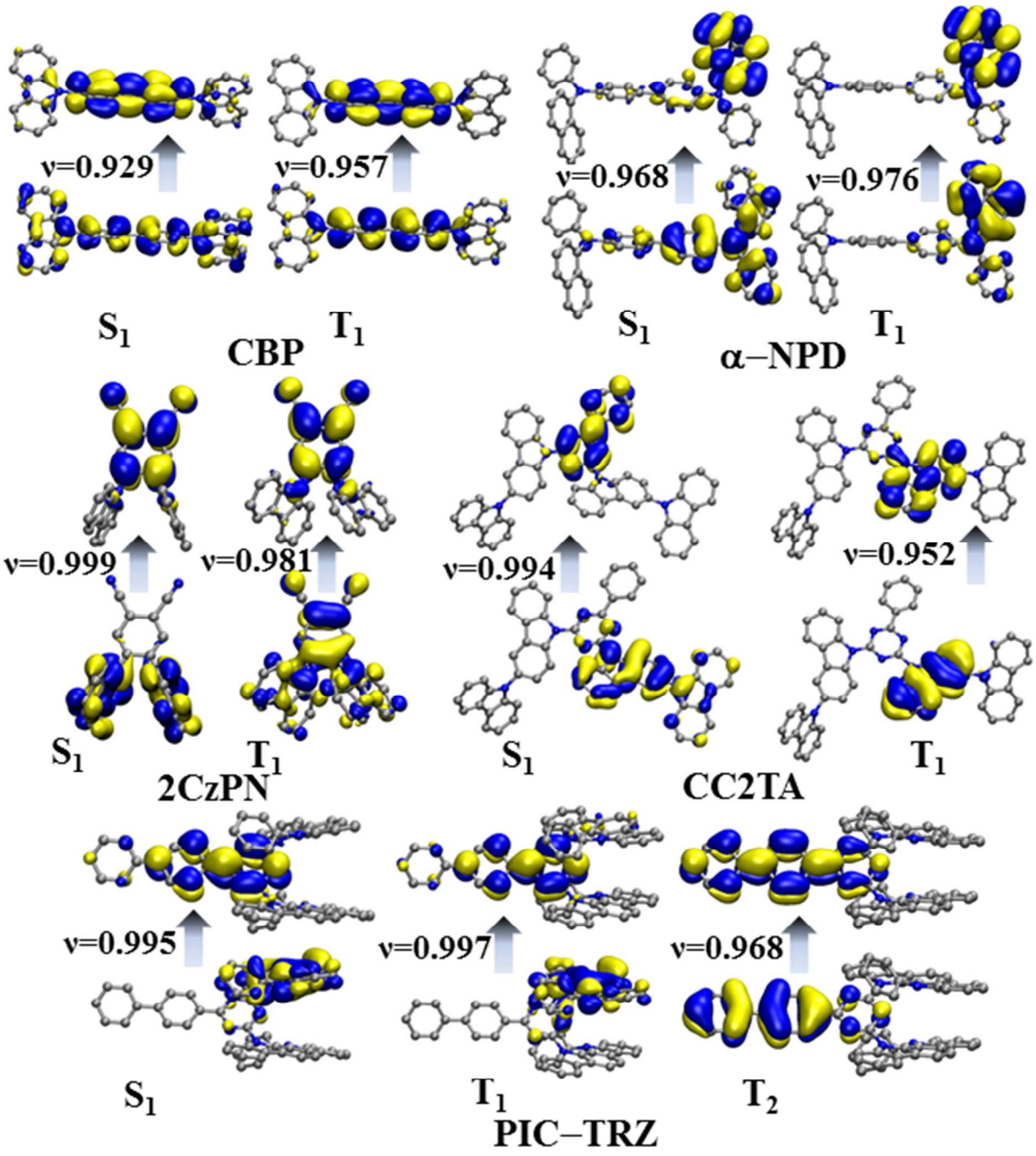

Figure S2. Natural Transition Orbitals of CBP, α-NPD, 2CzPN, CC2TA, and PIC-TRZ corresponding to the S_1 and T_1 states at their respective optimized geometry (the T_2 state is also included for PIC-TRZ). Hole and electron wave functions with the largest weight, ν, are illustrated below and above the arrows, respectively. Hydrogen atoms are omitted for the sake of clarity.

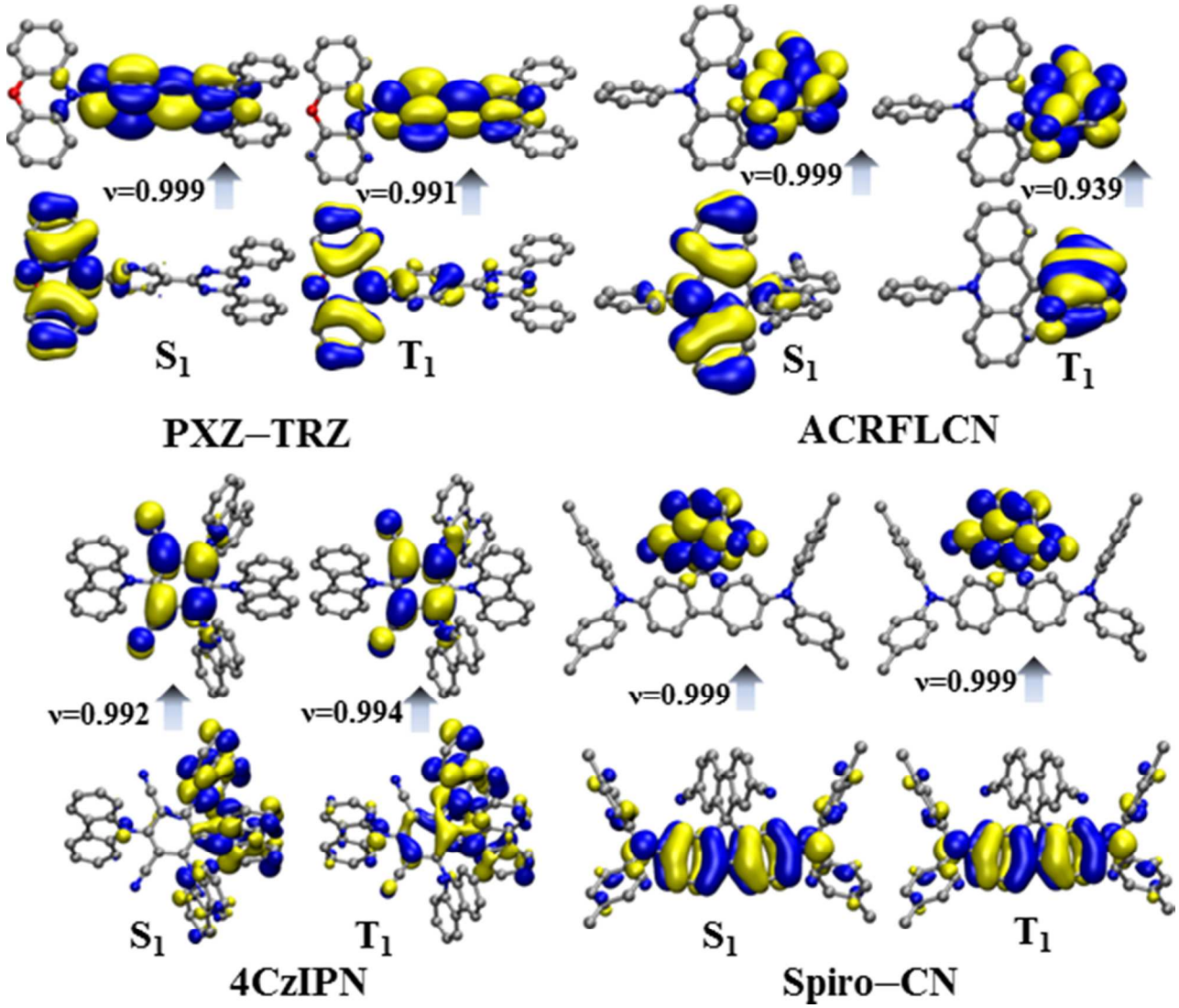

Figure S3. Natural transition orbitals of PXZ-TRZ, ACRFLCN, 4CzIPN, and Spiro-CN corresponding to the S_1 and T_1 states at their respective optimized geometry. Hole and electron wave functions with the largest weight, ν, are illustrated below and above the arrows, respectively. Hydrogen atoms are omitted for the sake of clarity.

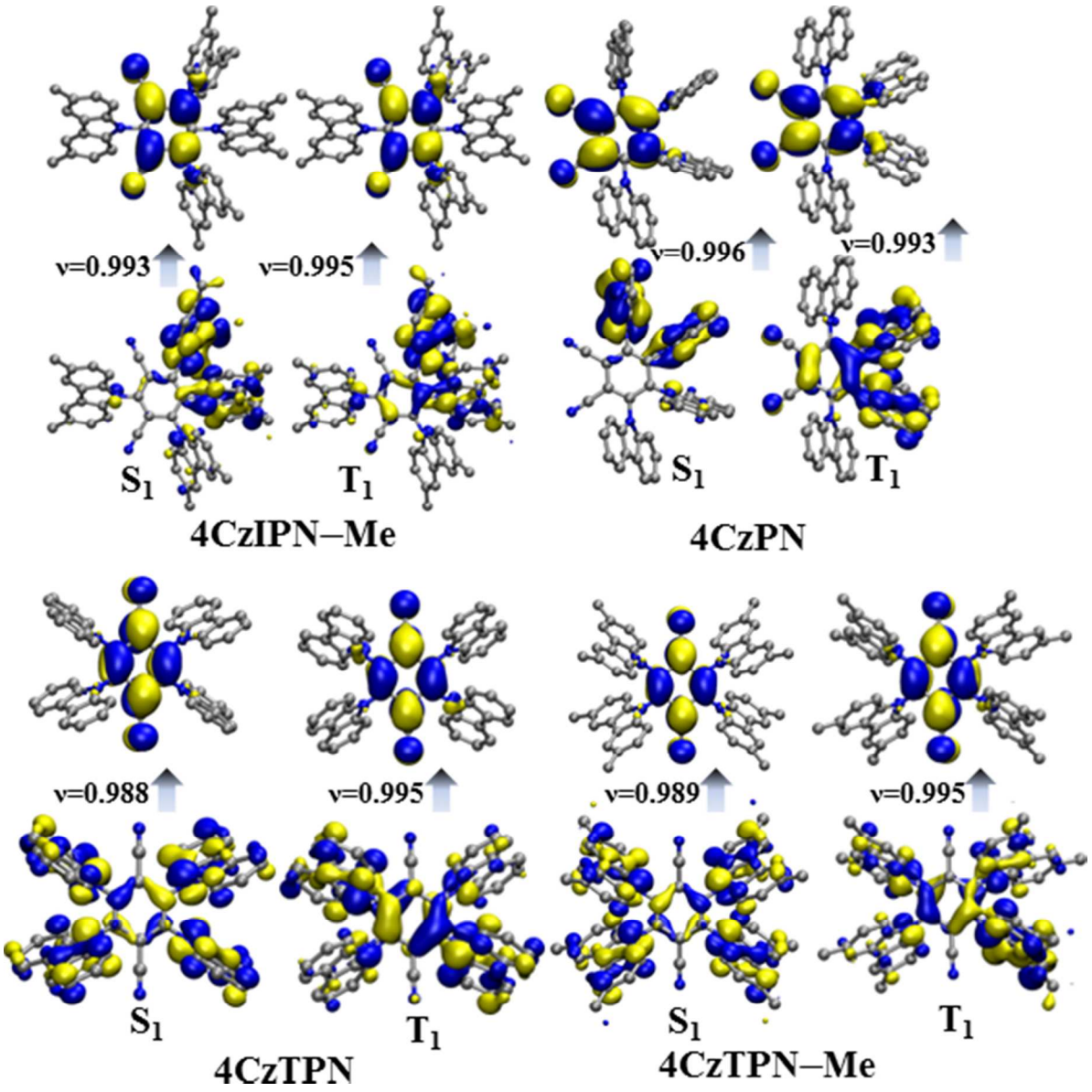

Figure S4. Natural transition orbitals of 4CzIPN-Me, 4CzPN, 4CzTPN, and 4CzTPN-Me corresponding to the S_1 and T_1 states at their respective optimized geometry. Hole and electron wave functions with the largest weight, ν, are illustrated below and above the arrows, respectively. Hydrogen atoms are omitted for the sake of clarity.

2. References

(1) Baer, R.; Livshits, E.; Salzner, U. *Annu. Rev. Phys. Chem.* **2010**, *61*, 85.

(2) Refaely-Abramson, S.; Baer, R.; Kronik, L. *Phys. Rev. B* **2011**, *84*, 75144.

(3) Kronik, L.; Stein, T.; Refaely-Abramson, S.; Baer, R. *J. Chem. Theory Comput.* **2012**, *8*, 1515.

(4) Refaely-Abramson, S.; Sharifzadeh, S.; Govind, N.; Autschbach, J.; Neaton, J. B.; Baer, R.; Kronik, L. *Phys. Rev. Lett.* **2012**, *109*, 226405.

(5) Srebro, M.; Autschbach, J. *J. Chem. Theory Comput.* **2012**, *8*, 245.

(6) Sun, H.; Autschbach, J. *Chemphyschem* **2013**, *14*, 2450.

(7) Levy, M.; Perdew, J. P.; Sahni, V. *Phys. Rev. A* **1984**, *30*, 2745.

(8) Sun, H.; Zhong, C.; Brédas, J. L. *J. Chem. Theory Comput.* **2015**, *11*, 3851.

(9) Bokareva, O. S.; Grell, G.; Bokarev, S. I.; Kühn, O. *J. Chem. Theory Comput.* **2015**, *11*, 1700.

(10) Lu, T.; Chen, F. *J. Comput. Chem.* **2012**, *33*, 580.

(11) Kim, D. *J. Phys. Chem. C* **2015**, *119*, 12690.

(12) Brédas, J. L.; Beljonne, D.; Coropceanu, V.; Cornil, J. *Chem. Rev.* **2004**, *104*, 4971.

(13) Schmidt, K.; Brovelli, S.; Coropceanu, V.; Beljonne, D.; Cornil, J.; Bazzini, C.; Caronna, T.; Tubino, R.; Meinardi, F.; Shuai, Z.; Brédas, J. L. *J. Phys. Chem. A* **2007**, *111*, 10490.

(14) Barbara, P. F.; Meyer, T. J.; Ratner, M. A. *J. Phys. Chem.* **1996**, *100*, 13148.

(15) Reimers, J. R. *J. Chem. Phys.* **2001**, *115*, 9103.

(16) Beljonne, D.; Shuai, Z.; Pourtois, G.; Brédas, J. L. *J. Phys. Chem. A* **2001**, *105*, 3899.

(17) Huang, S.; Zhang, Q.; Shiota, Y.; Nakagawa, T.; Kuwabara, K.; Yoshizawa, K.; Adachi, C. *J. Chem. Theory Comput.* **2013**, *9*, 3872.